Journal of Applied Fluid Mechanics, Vol. 16, No. 9, pp. 1704-1716, 2023.
Available online at www.jafmonline.net, ISSN 1735-3572, EISSN 1735-3645.
https://doi.org/10.47176/jafm.16.09.1792

Numerical Investigation on Separation Efficiency of a Novel Hybrid Engine Air-Particle Separator

S. Ghodbane[1,3], A. Beniaiche[2], A. Belkallouche[3] and B. Janssens[4†]

[1] *Laboratory of Propulsion and Reactive Systems, Ecole Militaire Polytechnique, BP17 Bordj-el-Bahri, 16046 Algiers, Algeria*
[2] *Laboratory of Fluid Mechanics, Ecole Militaire Polytechnique, BP17 Bordj-el-Bahri, 16046 Algiers, Algeria*
[3] *Ecole Supérieure des Techniques de l'aéronautique, Dar El-Beida, Algiers, Algeria*
[4] *Royal Military Academy RMA, Brussels, Belgium*

†Corresponding Author Email: bart.janssens@mil.be

ABSTRACT

This paper proposes a novel design for a hybrid engine air-particle separator filter (HEAPS) that combines the vortex tube separator (VTS) with the inertial particle separator (IPS) to enhance separation efficiency. Helicopters often operate in harsh environments, such as deserts, and landing on unprepared runways poses a severe risk to turboshaft engines due to the ingestion of dust and sand. This can result in significant damage to the engine's rotating components, impacting its life, reliability, and performance. To protect the engine from erosion and damage, an engine air particle separator system (EAPS) is installed in the engine inlet. In this study, a comparative numerical simulation was conducted between the hybrid filter and the VTS using the commercial software ANSYS Fluent. The Reynolds-averaged Navier–Stokes equations (RANS) were used to simulate incompressible turbulent flow, and the trajectory of particles was tracked using the Discrete Phase Model (DPM). Particle trajectories and separation efficiency were analyzed for different particle sizes, inlet velocities, and bypass mass flow ratios between the scavenge channel and the core engine channel. The results show that the hybrid design provides excellent separation efficiency, with a recovery efficiency of over 97%.

Article History

Received January 29, 2023
Revised April 6, 2023
Accepted April 20, 2023
Available online July 1, 2023

Keywords:

Innovative hybrid filter geometry
Vortex tube separator
Inertial particle separator
Separation efficiency
Discret phase model

1. INTRODUCTION

The operation of helicopters in brown-out situations (as shown in Fig. 1), where visibility near the ground is lost due to the cloud of sand lifted by the rotors, can cause significant damage to the engine. This includes erosion of the compressor blades, glazing of the combustion chamber walls and turbine. As a result, the engine's performance parameters, such as isentropic efficiency and pressure ratio, may decrease (Alqallaf & Teixeira, 2022). When the engine compressor and turbine are affected, it leads to a decrease in propulsive efficiency or shaft power and an increase in the temperature of the combustion chamber. To protect engine components from erosion and deterioration, engine air particle separators (EAPS) are installed on helicopter engines (Tabakoff & Hamed, 1984). Erosion is dependent on the particle's composition, velocity, and impact angles (Hamd et al., 2006). Understanding the significance of particle separators on modern helicopters requires examining performance data. For example, a light utility

helicopter with an engine mass flow of 5.9 kg/s, aspirating air with a particle mass concentration of 2.5 g/m³, absorbs about 0.7 kg of sand per minute (Van der Walt & Nurick, 1995a, 1995b). For an engine of this size, it can lose one percent of power after ingesting just 7 kg of particulate or operating for only ten minutes in a typical brownout cloud (Bojdo, 2012).

Prinsloo et al. (1991) showed the impact of inlet system modifications on engine performance, stating that "If the separation efficiency of the inlet system increases from 94% to 95%, the life expectancy of the engine is doubled, and if the efficiency then increases to 97%, the life expectancy is doubled again." The quote highlights the significance of improving the separation efficiency of the engine air particle separator (EAPS) system to extend the engine's life.

Nomenclature

C_D	drag force coefficient	Pt_e	inlet engine averagetotal pressure
d	particle diameter	Pt_i	inlet filter average total pressure
dt	time step	Re	Reynolds number
d	average diameter	Up	particle velocity
F_B	centrifugal force	Uf	fluid velocity
F_D	drag force	ρ	*air* velocity
m_i	total mass of particles entering the filter	ρ_p	particle density
m_p	particle mass	η	separation efficiency
m_s	total mass of particles entering the scavenge	ΔP	pressure drop
n	spread parameter	σ	total pressure recovery coefficient

2. BACKGROUND

2.1 Different Categories of EAPS

A critical component that protects the engine from sand and dust in the air is situated between the engine and the contaminated environment. There are three main types of Engine Air Particle Separation (EAPS) devices:

Inlet Barrier Filters (IBF), which use a mesh to capture particles in front of the inlets (Fig. 2. a).

Inertial Particle Separators (IPS), which rely on changes in the inlet geometry curvature. The IPS's main components are shown in Fig. 2. b. The two-phase flow of particle-laden air makes a turn at the aft of the hub, causing the particles to follow their path to the outer wall of the IPS due to their inertia. The clean air follows the hub's direction change and flows into the engine channel. Downstream of the hub, the clean air follows the turn to the engine channel, and the particles are scavenged away from the engine channel and ejected into the atmosphere.

Vortex Tube Separators (VTS), which separate particles by swirling the intake flow. Centripetal forces cause particles to move outward from the vortex, and they can be collected by diverting this outward flow to a secondary stream. In most applications, fixed helical vanes passively impose the vortex motion (Fig. 2. c).

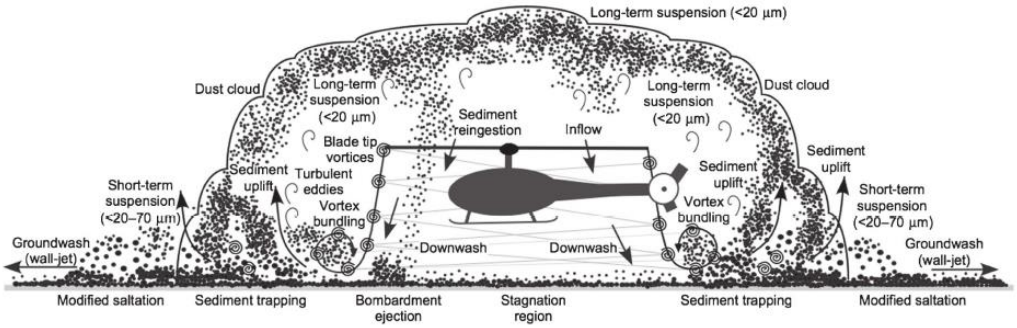

Fig. 1. A schematic of in-ground-effect aerodynamics and the brownout landing (Milluzzo & Leishman 2010).

(a) Inlet Barrier Filters (IBF)

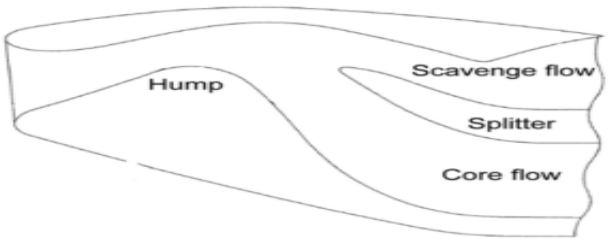

(b) Inertial Particle Separators (IPS)

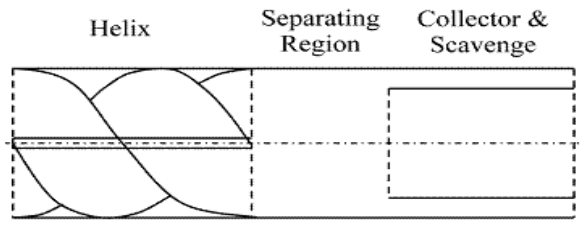

(c) Vortex Tube Separators (VTS)

Fig. 2. Engine air particle separator.

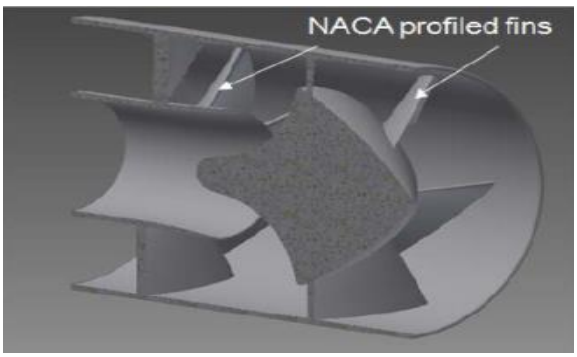

Fig. 3. Hybrid design of students of the University of Miami (Cozier et al., 2015).

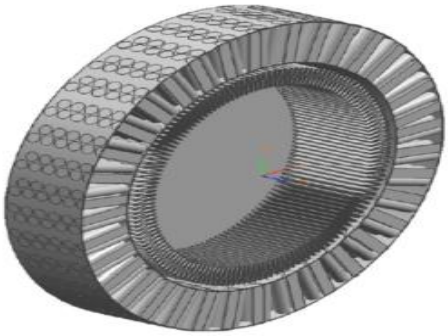

Fig. 4. Hybrid design of (VTS + IBF) (Bojdo & Filippone 2017).

The efficiency of EAPSs is affected by various factors, including inlet velocities, particle diameter, bypass mass flow of the scavenge, and geometrical parameters that are specific to each concept (Filippone & Bojdo 2010). For IPS, geometrical factors such as the geometry of the outlet surface (OSG), the hub, and splitter play a significant role in determining its performance (Connolly et al., 2023). Meanwhile, Gopalakrishnan (2019) found that the separation efficiency and pressure drop of VTS are primarily influenced by the number and angle of helixes, the vortex generator length, and the separation zone length.

The IBF concept shows superior separation efficiency and pressure losses compared to other concepts. This design employs a filter element to trap particles in the incoming air, allowing only clean air to enter the engine. Over time, as particles accumulate on the filter element, the separation efficiency improves, but this comes at the cost of increased pressure drop. To prevent potential engine damage from foreign objects, a bypass door controlled by a pilot opens when the pressure drop reaches a critical value (Daldal, 2023).

There have been few studies on hybrid filters, and one such study is the work by Cozier et al (2015) from the University of Miami. They developed a hybrid filter that combines the inertial particle separator with the vortex tube separator, with their IPS design inspired by Hobbs (1983) and reinforced with NACA profile obstacles, as shown in Fig. 3. Experimental results demonstrated that their hybrid filter achieved a separation efficiency of 79.3% for MIL-STD-810G test dust with sand sizes ranging between 10 and 200 μm. However, their study did not account for the impact of varying inlet velocities, particularly low velocities, and the bypass between the engine mass flow and the scavenge mass flow on the system's performance.

Another hybrid concept was developed by Bojdo & Filippone (2017), which combines the advantages of the inlet barrier filter and vortex tube separator devices, as shown in Fig. 4. The first stage consists of the VTS, followed by the IBF in the second stage, which captures the small particles that passed through the VTS. The authors modified the distribution of particle sizes of the AFRL 02 test dust and achieved a separation efficiency of up to 90.6%. However, using two stages of filters increases the weight of the helicopter. One of the drawbacks of the IBF is its susceptibility to clogging in conditions where sand is present in large quantities, increasing the risk of engine damage and additional maintenance costs (Filippone & Bojdo 2010).

2.2 Vortex Tube Separator

The Vortex Tube Separator (VTS) is a commonly used engine protection system for helicopters operating in desert environments. The design of the VTS in this study was inspired by the geometry of the VTS from Pall Aerospace **(**Stallard, 1997**)**, as shown in Fig. 5. The particle-laden air is swirled by the static helix, which imparts a radial acceleration to the particles. The particles achieve a steady-state radial acceleration equal to their terminal velocity, and the drag force induced by the relative velocity is balanced by the radial force field. Downstream of the helix is the separation region, where the particles have time to reach the outer annular region of the flow, which is eliminated by scavenging, while the clean air enters the engine. The main geometrical parameters of the design (Fig. 6) are the helix angle of 180 degrees, four blades, outer and inner tube diameters, and axial distance between the helix and the collector, all chosen to improve separation efficiency.

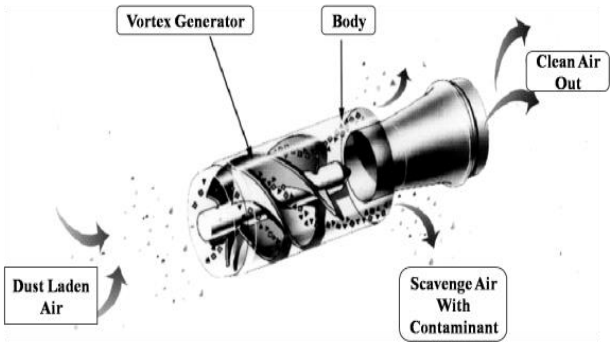

Fig. 5. Skech of VTS (Stallard, 1997).

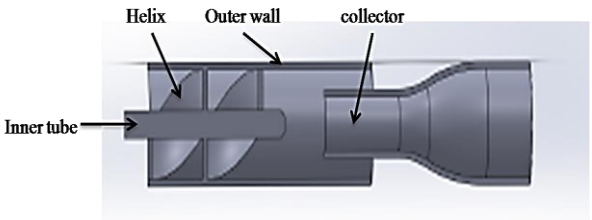

Fig. 6. Vortex Tube Separator view section.

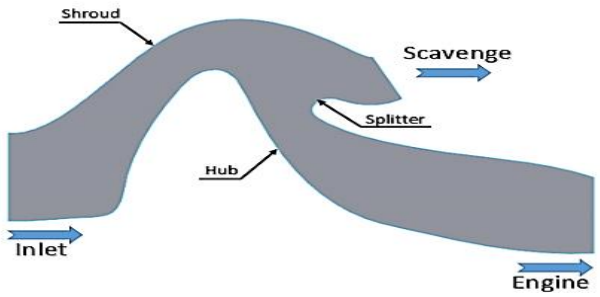

Fig. 7. Inertial Particle Separator.

2.3 Inertial Particle Separator

The Inertial Particle Separator (IPS) operates by inducing a rapid change in the curvature of the HUB geometry. As the two-phase flow enters the IPS filter, it follows the HUB shape to its peak, where the flow makes a sudden turn. Due to their inertia, most of the particles are unable to turn with the flow and are thrown radially toward the outer wall, exiting through the scavenge channel. On the other hand, the clean air successfully makes the turn and enters the engine channel (Fig. 7).

The separation efficiency of the particles in the IPS filter is significantly affected by its geometrical parameters. In a study conducted by Ghenaiet & Tan (2004), the effect of hub change, splitter, and scavenge channel near walls on particle separation performance in RTM322 engines was numerically investigated.

2.4 The New Proposed Hybrid Design

The design incorporates the inertial particle separator concept into the central supporting axis of the vortex tube, where the helix and the hub are configured coaxially and encircled by a horizontal shroud. The hub forms an annular channel of decreasing area with the encircling shroud, creating a rotating motion with increasing velocity of the flow (air+particles) induced by its helix. The radius of the hub rises in the axial direction from the inlet to a peak and then decreases towards the engine channel inlet. The shape of the shroud in the separation zone is curved. Two helical blades are used in the design, which is a reduction compared to the VTS with four helixes. Each helix has a chord length of at least 180 degrees measured across the tube circumference to ensure that each particle is subjected to a swirling force, either aerodynamically or by direct deflection. Figure 8 illustrates the new design.

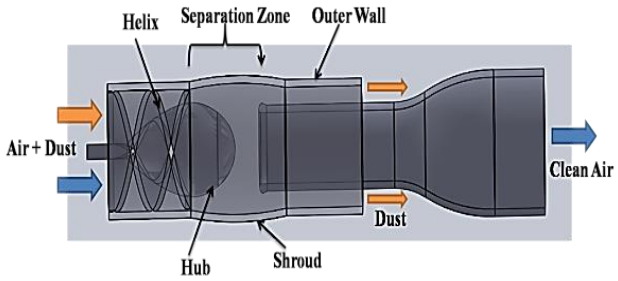

Fig. 8. New filter Hybrid Design

3. THEORY

Using a Lagrangian method, the particle force balance equation is solved to provide the particle trajectories. A particle ("p") is identified by the position of a particle's center (x,y,z), diameter (d), density (ρ) and velocity (u,v,w). The particle has the following mass:

$$m_p = \frac{1}{6}\rho_p \pi d^3 \tag{1}$$

The equation for determining particle location x_p in a Lagrangian frame is:

$$\frac{dx_p}{dt} = u_p \tag{2}$$

The Newton's equation defines the motion of particles:

$$m_p \frac{d\boldsymbol{u_p}}{dt} = \sum \boldsymbol{F} \tag{3}$$

After the particles come into contact with the helix, their trajectory changes and becomes helical. When leaving the vanes, the velocity of the particles can be decomposed into three components (Dziubak et al., 2020):

- u_s the tangential particle velocity ,
- u_r the radial particle velocity ,
- u_x the axial particle velocity.

The forces acting on the particles include the centrifugal force F_B, the aerodynamic force F_R, and the buoyancy force F_G. These forces are influenced by various factors such as the particle's size, shape, composition, and the medium in which it exists.

The aerodynamic force exerted on a particle is the net force exerted on the particle due to the surrounding fluid. This force is influenced by various factors, such as the particle's size, shape, velocity, and the fluid properties such as density and viscosity. It is given by the following equation:

$$\boldsymbol{F_R} = \boldsymbol{F_D} + \boldsymbol{F_L} + \boldsymbol{F_{gr}} \tag{4}$$

Where :

$\boldsymbol{F_D}$ is the drag force; $\boldsymbol{F_L}$ the Lift force and $\boldsymbol{F_{gr}}$ the gravity force.

In the case of a "fine" particle, where the gravity force is negligible compared to the other forces, we can assume $F_{gr} = 0$.

This assumption is often reasonable for small particles. If we assume that the particle or object is a perfect sphere, the lift force can be neglected, ($F_L = 0$). This assumption simplifies the calculation of the flow around the object. By making these assumptions, equation (4) becomes:

$$F_R \approx F_D \tag{5}$$

The most dominant force exerted on a particle in a dilute flow is the drag F_D of the fluid phase: we ignore the Magnus force in situations where there is no shear flow. And we neglect other forces like the added mass,

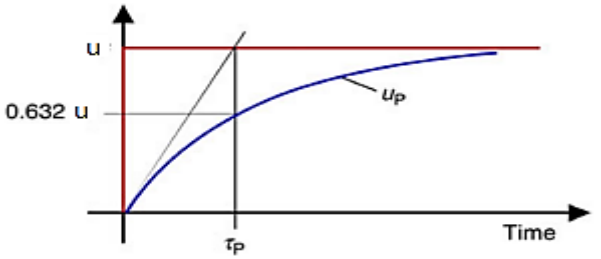

Fig. 9. Graphical illustration of the particle response time (Sommerfeld, 2011).

the buoyancy force and the Basset history term because the density of particles is significantly higher than that of the carrier gas, i.e., $\rho_p \gg \rho_g$.

Using Newton's principle in the radial direction yields:

$$\sum F = F_B - F_R = m_p \frac{du_r}{dt} \tag{6}$$

After the particles come into contact with the helix, a swirling motion is created, resulting in a centrifugal force that depends on the particle mass, m_p, and the radius, "r," of this rotational motion (Song et al., 2017) :

$$F_B = m_p \frac{u_s^2}{r} = \frac{1}{6}\rho_p \pi d^3 \frac{u_s^2}{r} \tag{7}$$

The particle Reynolds number is given by (Bojdo & Filippone, 2017),

$$Re_p = \frac{\rho_f d(u_f - u_p)}{\mu_f} \tag{8}$$

Where u_f is the fluid velocity, $\mu_f$is the fluid viscosity, and ρ_f is the fluid density. The drag force can be expressed as (Crowe et al., 1998)

$$F_D = -m_p \frac{u_p - u_f}{\tau_p} \tag{9}$$

The particle relaxation time τ_p represents the time taken for the particle to react to changes in the local velocity of the flow (Fig. 9).

when the drag coefficient C_D is defined as the following (Vallier, 2009):

Stokes regime :

$$C_D = \frac{24}{Re_p} \qquad if\ Re_p \geq 0.1 \tag{10}$$

Transition regime :

$$C_D = \frac{24}{Re_p}\left(1 + \frac{1}{6}{Re_p}^{2/3}\right) \text{ if } 0.1 < Re_p \leq 1000 \tag{11}$$

Newtonian regime:

$$C_D = 0.44 \qquad if\ \mathrm{Re_p} > 1000 \tag{12}$$

If the particles are extremely small, the flow field that surrounds the particle cannot be considered continuous. Due to the slip of the flow, a Cunningham factor "*C*" must be taken into account when calculating the drag force (Jennings, 1988).

$$C = 1 + Kn\left[2.514 + 0.8\, e^{-\left(\frac{0.55}{Kn}\right)}\right] \tag{13}$$

with the Knudsen number *Kn* is equal to:

$$Kn = \frac{\lambda}{d_p} \tag{14}$$

The mean free path of the gas molecules λ is given by:

$$\lambda = \frac{\mu}{0.499}\sqrt{\frac{\pi}{8\rho \mathrm{P_a}}} \tag{15}$$

Several parameters can affect the separation efficiency of EAPSs, including particle diameter, initial velocities, initial locations (i.e., whether particles are closer or farther from the inlet periphery), bypass scavenge flow, and filter geometry. Depending on whether a particle is more influenced by the centrifugal force $F_B$or the aerodynamic force F_R, it will either exit the scavenge channel or follow the predominant airflow into the engine channel.

The outlet face is divided into two sections: outlet 1, which represents the clean air, and outlet 2, which represents the scavenging face to the atmosphere. The separation efficiency (η) is defined as the ratio of the number of particles (N_2) leaving through outlet 2 to the total number of particles (N) entering the inlet filter:

$$\eta = \frac{N_2}{N} \tag{16}$$

The Stokes number (ST_L) provides a tool to compare the multiphase interactions and study a particle's response to the fluid flow field. The Domain Stokes number (Eq. 13) is defined as the ratio of the particle response time τ_p, given by the ratio of the particle's inertia to the drag force$\left(m_p u_p / F_D\right)$, and the domain fluid response time τ_e, which is the time required for a fluid element to pass through the domain (Barone et al., 2017):

$$ST_L = \frac{\tau_p}{\tau_e} \tag{17}$$

In particle-laden turbulent flows, the interaction between the particles and the fluid flow can be characterized by the dimensionless particle volume fraction $\phi_p$which is defined as the ratio of the volume occupied by the particles to the total volume of the fluid. It is given by:

$$\phi_p = \frac{N.V_p}{V} \tag{18}$$

Where: N is the number of particles; V_p the volume of a single particle and V is the total volume occupied by air and particles.

When the value of ϕ_p is very low ($\leq 10^{-6}$), the particles have a negligible effect on the fluid flow, and the interaction between the particles and the fluid can be considered as one-way coupling. In this regime, the particles are assumed to be small enough not to significantly alter the fluid flow, and the momentum transfer from the particles to the fluid is negligible. In other words, the particles are passively transported by the fluid flow, and their dispersion is determined solely by

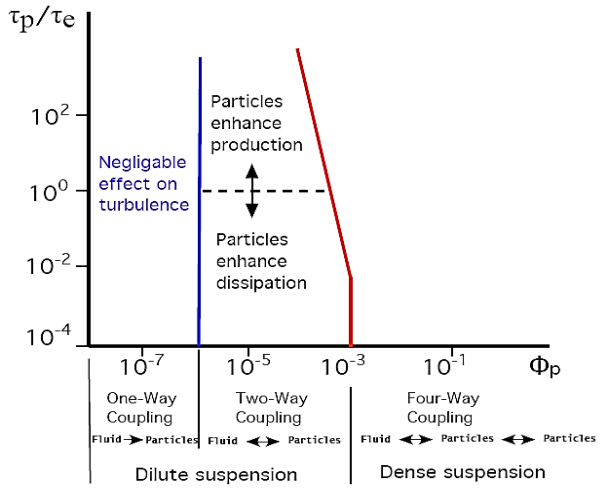

Fig. 10. Categorization of coupling schemes by (Elghobashi, 1994).

the characteristics of the fluid flow, such as turbulence intensity and length scales.

When the particle volume fraction exceeds 10^{-6}, particles significantly affect fluid flow, resulting in a phenomenon known as two-way coupling. This interaction leads to a significant momentum transfer from particles to fluid, causing alterations in the fluid flow through interactions with turbulent eddies. Elghobashi (1994) categorized this phenomenon, as shown in Fig. 10.

4. NUMERICAL PROCESS

The aim of this study was to develop a new particle separator design based on numerical predictions of the Hybrid VTS-IPS. This involved determining the trajectory of particles in the hybrid VTS-IPS, as well as pressure and velocity distribution. Additionally, the separation efficiency of the Hybrid VTS-IPS was evaluated with regard to inlet velocity, particle size, and bypass value. To simulate airflow with particles using the Hybrid VTS-IPS, the following table 1 resumes utilized input data:

The numerical simulation was conducted using the ANSYS FLUENT software. The k-ω SST RANS approach was employed to solve the flow field, and discrete phase modeling (DPM) was utilized to calculate particle trajectories through Lagrangian solvers. All calculations were performed for an incompressible fluid.

Table 1 Simulation's imput values.

Input	value
Mineral dust	SiO_2
Particle density ρ_p	2650 kg/m^3
Air density ρ	1,225 kg/m^3
Air dynamic viscosity μ	1,785.10^{-5} Ns/m^2
Air kinematic viscosity υ	1,471.10^{-5} m^2/s
Air ambient temperature T_a	15°C
Air ambient pressure P_a	1,013.10^5 Pa

The simulation aimed to compare the new hybrid filter with the baseline VTS in terms of separation efficiency versus bypass flow. Bypass flow refers to the ratio between the mass flow entering the scavenge $\dot{m}_s$ channel and the mass flow entering the inlet filter $\dot{m}_\iota$.

$$Bypass = \dot{m}_s/\dot{m}_\iota \quad (19)$$

Since the scavenging flow rate should be less than approximately 10% (Bojdo & Filippone 2012), we selected three different values: 2%, 6%, and 10%. When selecting a coupling method for particle flow analysis in ANSYS, various factors can be taken into account, including computational efficiency, differences in time scales, and the weak interaction between the particles and the medium. Based on the given information, the simulation involves a particle volume fraction of less than 10^{-6}, suggesting that one-way coupling is sufficient to approximate the impact of turbulence on particle behavior.

4.1 Particle Characteristics and Size

For the physical characteristics of the dust particles, the following simplifying assumptions have been made:

- The particles are assumed to be spherical in shape to eliminate the effects of particle shape.
- The dominant aerodynamic force acting on the particles is considered to be the drag force.
- The Lagrange equations are used to calculate the particle trajectories.
- The particles are assumed to be small enough that they do not significantly affect the flow characteristics.
- The material of the particles is determined by assigning a specific density.
- The particle-wall interactions are defined as follows:
  - "Reflect": This is achieved by using a "wall" boundary condition with the "reflection" in DPM option enabled, which models the wall as perfectly reflecting. The wall is defined as a no-slip surface to ensure that particles experience a change in velocity upon impact with the wall.
  - "Trap": For a "trap" interaction, a boundary condition that models the wall as an absorbing or sticky surface is typically used, so that particles are unable to escape. This can be achieved using a "trapped" boundary condition in the simulation.
  - "Escape": This refers to a situation where a particle being tracked in a simulation has exited the simulation domain or has reached a condition where it is no longer being tracked, resulting in a defined number of non-filtered particles.

As the problem of particle ingestion is more severe for fine particles due to their low inertia, we have selected the following particle size distributions:

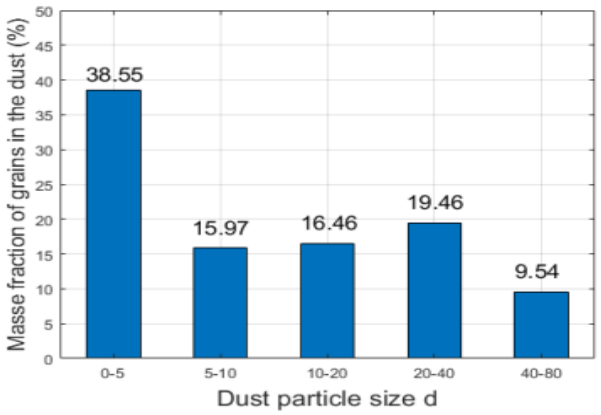

Fig. 11. Dust sizes of PTC-D test dust (Dziubak et al., 2020).

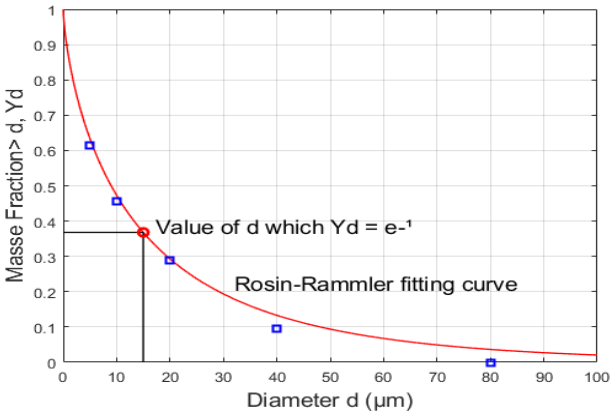

Fig. 12. Diameter distribution curve by the Rosin Rammler method.

- Seven monodisperse dusts with particle diameters of 2, 5, 10, 15, 20, 25, 50, and 80 µm.
  - One polydisperse particle model using the Rosin Rammler distribution Y_d, which is calculated using the formula outlined in the Fluent ANSYS (2019).
  - $Y_d = e^{-(d/\bar{d})^n}$ (20)

Where n represents the spread parameter; d represents the particle diameter and $\bar{d}$ represents the average diameter. The average diameter is the value of the diameter for which $Y_d \approx 0.3681$.

The spread parameter n for the Rosin Rammler distribution can be calculated using the following relation:

$$n = \frac{\ln(-lnY_d)}{\ln(d/\bar{d})} \quad (21)$$

In the present work, simulations are carried out utilizing the PTC-D test dust, as shown in Fig. 11. This dust is commonly used as a national substitute for the AC fine test dust (PN-ISO 5011 1994).

The parameters for the Rosin Rammler distribution of particles were calculated using formulas 20 and 21. Based on Fig. 12, the determined values were Y_d = 0.368, n = 0.715 and d = 15 µm. The simulated particle diameters were chosen from a distribution ranging from 1 to 80 µm, with a selection of (5) different diameters.

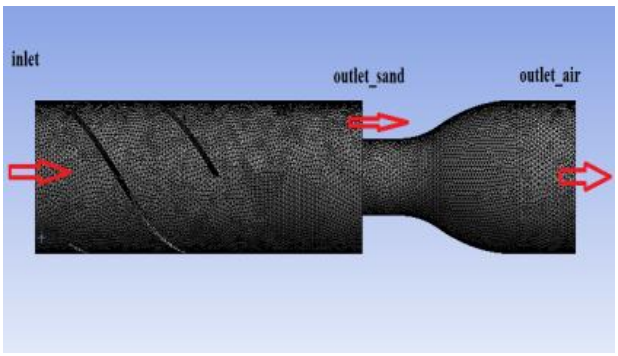

(a) Mesh of VTS

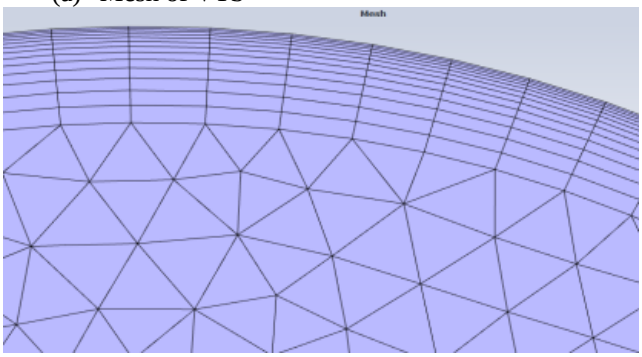

(b) Sublayer meshing

Fig. 13. Meshing of filters.

4.2 Mesh and Boundary Conditions

An unstructured mesh consisting of tetrahedral elements was utilized in the simulation. A total of 20 layers were uniformly applied to the hybrid filter walls and VTS walls, as depicted in Fig. 13(a, b). The mesh was refined in the viscous sublayer to meet the requirements of the kω-sst turbulence model. This ensured that the turbulent boundary layer was fully resolved, with a dimensionless wall distance (Y+) less than unity, as illustrated in Fig. 13(b). The Y+ parameter is a crucial factor in the outcomes, particularly the pressure losses resulting from wall friction in helix systems, as previously noted by Saberi (2014).

A numerical analysis was conducted to ensure a mesh-independent solution for the simulation. The mesh size of the VTS was varied, and the pressure drop across the filter was evaluated for each size. Figure 14 illustrates the results of the analysis. The pressure drop values were compared and found to vary by less than 1% between mesh sizes of 1,04 millions elements and 3,67 millions elements. A mesh size of 1 044 415 elements was selected for simulating the VTS filter, which corresponded to a grid element size of 0.5 *mm*. For HEPA filters, which have the same element size, the number of grid elements is 1 126 235.

Regarding the boundary conditions applied to the particles, a uniform projection is used to direct them towards the filter inlet plane, and a reflection condition is applied. The particles are subjected to a reflection-collision condition upon contact with the walls, and a no-slip shear condition is applied. Additionally, an escape boundary condition is applied at the engine channel outlet for the sand particles, and a trapped

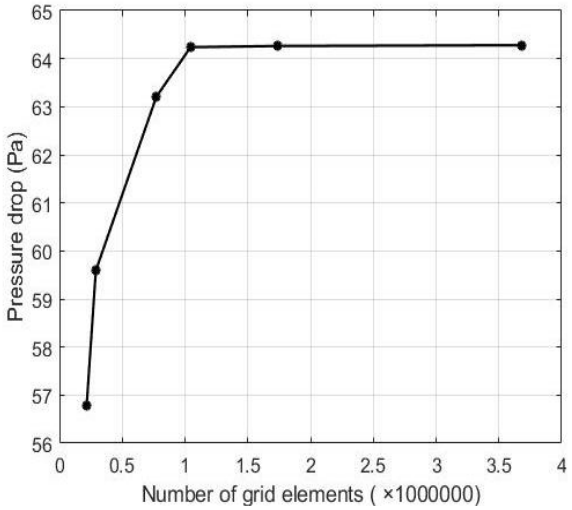

Fig. 14. Mesh independence study.

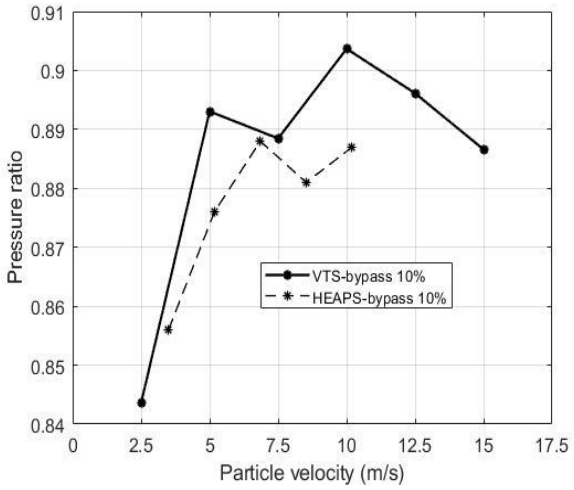

Fig. 15. Comparison of VTS separation efficiency between simulations results and experimental results by Dziubak (2020). (PTC-D dust sizes and bypass = 10%).

boundary condition is applied at the scavenge channel outlet for the air particles (Fig. 13. a).

5. RESULTS AND ANALYSIS

The analysis method selected for the simulation was one-way-coupled, using the ANSYS program. The flow field was initialized with an inlet velocity (v_0) range of 2.5-15 *m/s* and bypass values of 2%, 6%, and 10% in the outlet sand.

In order to assess the accuracy of the numerical model, a comparison was made between the simulation results and experimental data gathered by Dziubak (2020). As seen in Fig. 15, the separation efficiency of the VTS filter for PTC-D test dust with a 10% bypass showed excellent agreement with the experimental results, with a maximum error rate of less than 1%.

5.1 Pressure Drop

The pressure drop occurring in the innovative filter and the VTS filter was studied in the flow field as it directly affects engine performance. The pressure loss was evaluated using the total pressure recovery coefficient, which is defined as the ratio between the average total pressure at the engine inlet and the average total pressure at the filter inlet. The coefficient is expressed as follows, as described by Zhou et al. (2019):

$$\sigma = \frac{P_{te}}{P_{ti}} \tag{22}$$

At a velocity of v_0=2.5m/s and bypass=6%, in the VTS filter (shown in Fig.16.a), the pressure drop is observed to increase as the air from the helix approaches the outlet. The pressure loss increases in the helix zone along the inner tube, which represents the center of the swirling motion, and also on the helix surface. These pressure drops are caused by the friction of the air on the walls. Downstream of the swirl motion, the pressure drop is further increased, particularly in the engine channel, due to the wake created behind the turbulence.

Figure 16b displays the total pressure recovery coefficient for a VTS-IPS hybrid filter under the

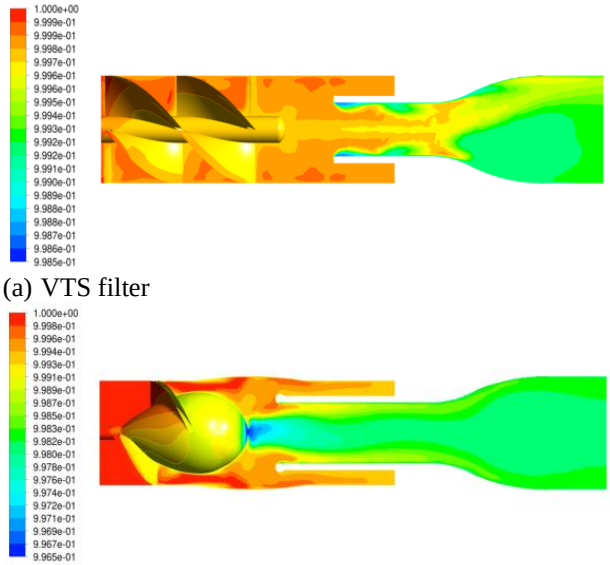

(a) VTS filter

(b) Hybrid VTS-IPS filter

Fig. 16. Total Pressure Recovery Coefficient contours across the median plane (v_0=2.5m/s and bypass = 6%).

conditions of an inlet velocity of v_0=2.5m/s and a bypass of 6%.

The pressure drop increases at the helixes of the hybrid filter, reaching its maximum value just at the outlet of the hub with a coefficient of 0.9965. The maximum pressure loss occurs at the end of the hub geometry due to the wake and friction in this zone.

The pressure drop then decreases in the engine channel and especially in the diffuser section, which plays a vital role in reducing the pressure loss.

At the end of the channel, the total pressure recovery coefficient decreases to 0.9983. Higher helix angles lead to increased pressure drop and efficiency, as noted in previous studies (Gopalakrishnan, 2019). In the study,

Table 2 Total pressure recovery coefficient for v_0=2m/s.

Bypass (%)	σ (VTS)	σ (Hybrid VTS-IPS)
2	0.99936	0.998239
6	0.99941	0.998264
10	0.99945	0.998288

the same helix characteristics were used for both the VTS and the hybrid VTS-IPS filters.

For higher velocities, the pressure drop increases in both filters due to the increase in velocity of the turbulent flow. In this study, a fixed velocity of v_0 = 2 *m/s* was used, and the pressure drop was determined for different bypass percentages, which are resumed in Table 2.

It can be observed that as the bypass increases, the pressure drop decreases. Additionally, the pressure drops for VTS are slightly lower compared to HEPA filters.

5.2 Separation Efficiency

To calculate the filtration efficiency in this numerical simulation, the following equation is utilized:

$$\eta = \frac{N_{trapped}}{N_{tracked} - N_{incomplete}} \tag{23}$$

Such as :

$N_{trapped}$ iss the number of particles that are trapped in the filter, $N_{tracked}$ is the total number of particles that are injected into the system and $N_{incomplete}$ represents the number of incomplete particles

The results can be classified into two categories based on the size of the particles: very fine particles and fine particles. Figures (17 and 18) compare the separation efficiency of VTS and Hybrid VTS-IPS filters for particles with sizes ranging from 2 μm to 80 µm (d = 2 μm, 5 μm, 10 μm, 15 μm, 20 μm, 25 μm, 50 μm, 80 μm) and different bypass percentages.

The separation efficiency of very fine particles (as shown in Fig. 17) increases as the inlet velocity (v_0) increases and depends on the bypass value. The results indicate that the separation efficiency of the hybrid filter is superior to that of the VTS filter. For particle diameters of 2 µm, the HEAPS filter achieves separation efficiencies between η=55% to η=99% for higher velocities, whereas the separation efficiency of the VTS is very low, ranging from η=3% to η=12% for a velocity of v_0= 15 *m/s*. The improvement in the separation efficiency of the HEAPS filter compared to the VTS is significant, and the same trend is observed for particle diameters of 5 µm, 10 µm, and 15 µm.

In the case of the VTS, the very fine particles with small size and low inertia are carried along with the air stream due to their low centrifugal force. As a result, most of these particles follow the air stream as it exits the engine channel. On the other hand, in the hybrid filter, even though these particles have low inertia, they follow an upward trajectory along the HUB when they reach the end of the swirl zone. They then continue their path in a radial direction towards the periphery of the HEAPS before entering the scavenging channel.

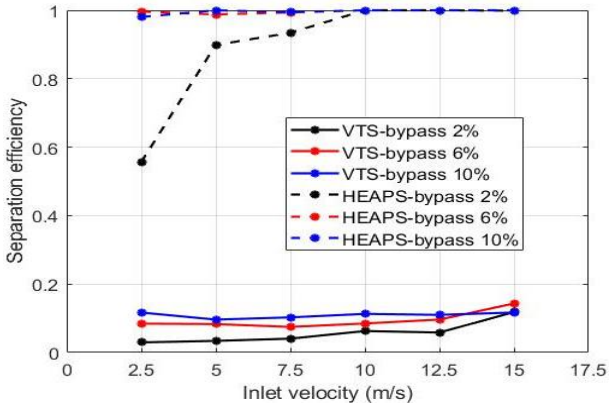

(a) d = 2 μm

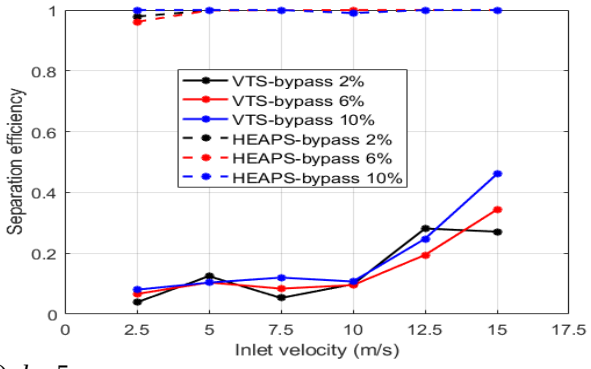

(b) d = 5 μm

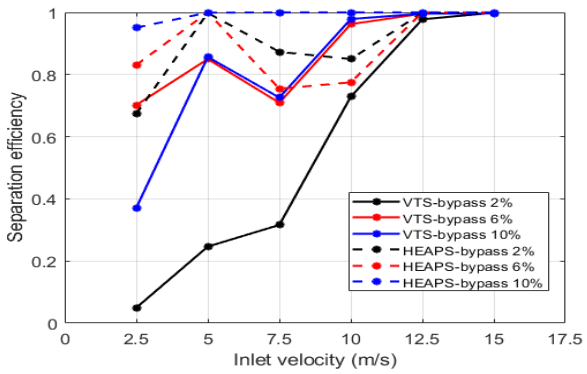

(c) d = 10 μm

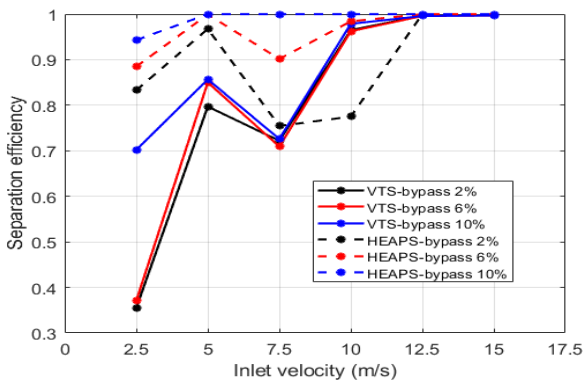

(d) d = 15 μm

Fig. 17. Comparison of Separation Efficiency for different sizes and bypasses of very fine particles.

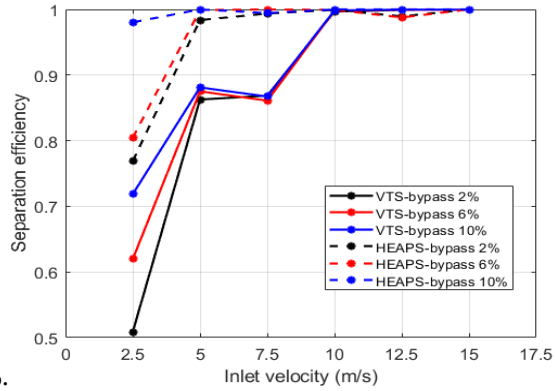

%.

(a) *d* = 20 *µm*

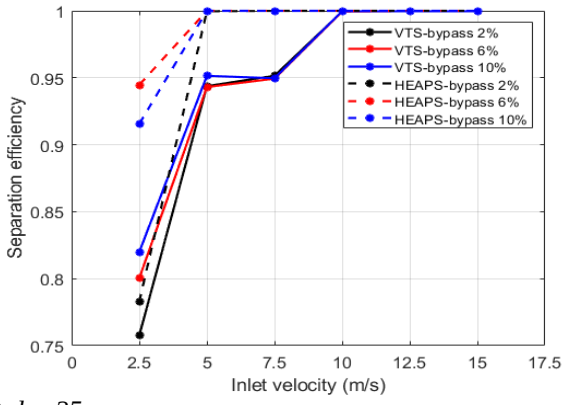

(b) *d* = *25 µm*

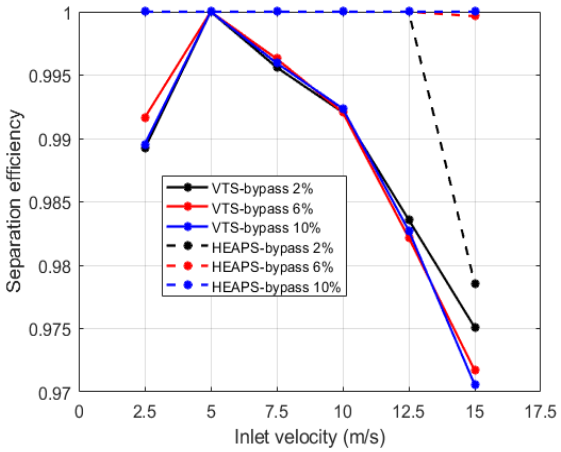

(c) *d=50 µm*

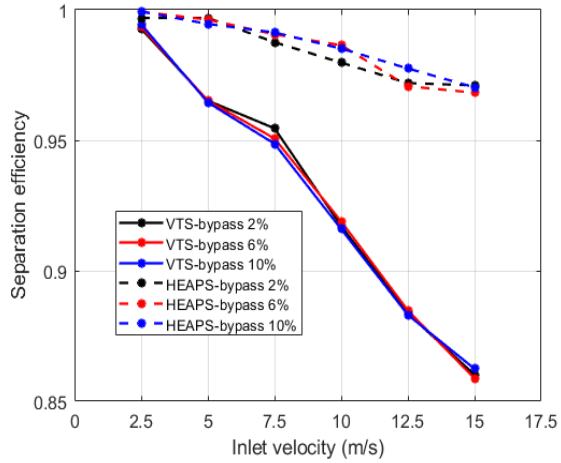

(d) d = 80 µm

Fig. 18. Separation Efficiency of fine particles.

Figure 18 shows the results of the separation efficiency of fine particles. The separation efficiency initially increases as the inlet velocity increases up to 10 *m/s*. However, beyond this velocity, the separation efficiency starts to decrease. This decrease can be attributed to the fact that heavier particles have a higher radial velocity, leading to more collisions and affecting their trajectory, thus decreasing the separation efficiency. Additionally, if the radial velocity is very small compared to the axial velocity, the axial component moves the particle forward and it follows a more outward path, leading to effective filtration. To reduce the rebound effect of heavy particles, the shroud in the separation zone of the innovative filter is curved compared to the VTS filter.

Figures 18.c and 18.d indicate that the separation efficiency of both the VTS and HEAPS filters varies for particles of 50 µm and 80 µm, as their trajectories differ from those of other particle diameters. The maximum separation efficiency of both filters (99%) is achieved at a low velocity of 2.5 *m/s*, but as the velocity increases, the separation efficiency gradually decreases. At a velocity of 15 *m/s*, the separation efficiency of the VTS and HEAPS filters are 86% and 96%, respectively. The drag force (F_D) has a significant impact on the centrifugal force (F_B) of the particles, and there is also likely a phenomenon of large dust particles reflecting off the filter walls. The HEAPS filter is less affected by this phenomenon than the VTS, probably due to the curved shape of its shroud.

For particles ranging from d = 20 µm to d = 80 µm, the Hybrid VTS-IPS filter consistently exhibits higher efficiency compared to the VTS filter, and both filters achieve an efficiency of over 95

In all of the aforementioned curves, increasing the bypass results in better separation efficiency due to the aspiration of flow in the scavenge channel by a pump. However, increasing the bypass also leads to a loss of engine power. Therefore, the bypass was limited to 10% based on the literature of Bojdo & Filippone (2012).

To investigate the impact of particle size on separation efficiency, particles of various diameters were injected into the inlet surface of both filters (innovative filter and VTS) individually. Figure 19 demonstrates the comparison of separation efficiency as a function of particle size for different inlet velocities and the VTS and Hybrid VTS-IPS devices. Both devices show a dependency on particle size, with the Hybrid filter outperforming the VTS by approximately 15%.

As the size of the particle increases, the component of the radial velocity also increases. This radial motion causes the particle to collide with the filter wall and rebound, leading to a decrease in separation efficiency. The rebound effect alters the anticipated trajectory of the particle, which is the filter periphery, and can cause it to deflect and enter the engine channel. Therefore, the rebound phenomenon plays a critical role in the particle's trajectory to the exit.

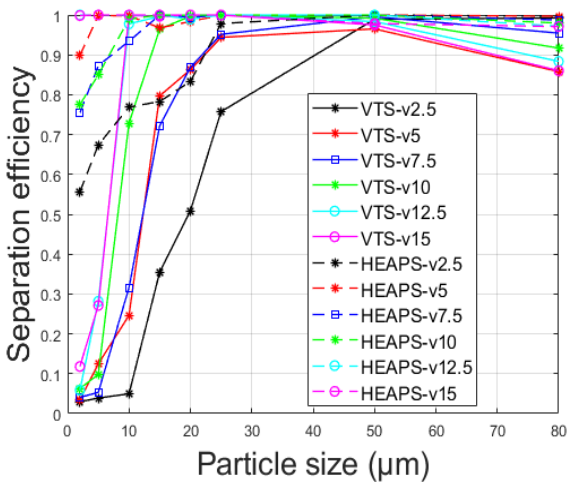

Fig. 19. The separation efficiency of different particle diameter.

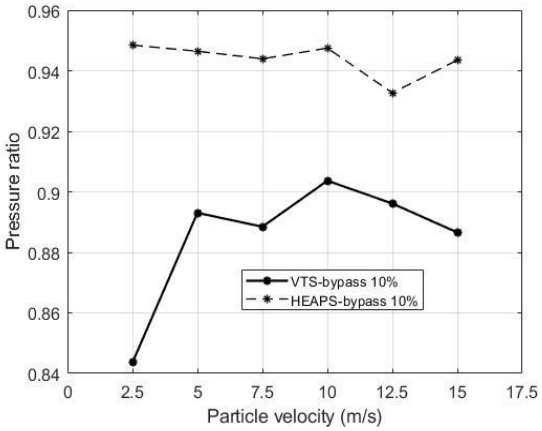

Fig. 20. Separation Efficiency of Rosin Rammler distribution.

Regarding the Rosin Rammler distribution (Fig. 20), the separation efficiency of the Hybrid VTS-IPS for a mix of particle diameters is approximately 94%, whereas that of the VTS ranges from 84% for a velocity of v_0 = 2.5 *m/s* to a maximum efficiency of 90% for v_0 = 10 *m/s*.

The Hybrid VTS-IPS filter exhibits superior particle separation performance compared to the VTS filter, particularly for particles with diameters of ($d \leq 15\ \mu m$ and $d \geq 50\ \mu m$). When air and dust enter the filters, the helixes induce a swirling motion to the particles and air. At the end of the filter helixes, particles with high inertia are directed towards the scavenge channel, while those with low inertia follow the air flow and enter the engine.

In the Hybrid VTS-IPS filter, the bi-phase flow encounters a change in the geometry of the IPS's Hub section at the end of the helixes. The clean air is guided by the Coanda effect towards the engine channel, while particles experience centrifugal force. Upon impact with the filter wall, sand and dust particles rebound and can re-enter the airflow. However, the change in direction of the Hub section helps low-inertia particles to continue towards the external wall and follow the wall geometry close to the scavenge channel, which decreases the rebound of the particles and leads to their exit to the outside. The rebound phenomenon results in a loss of initial energy for the particles, reducing their reflected velocity to below the inlet velocity.

Due to its effective particle separation capabilities, including the separation of very fine particles, the new HEAPS filter can operate in a single-stage array rather than requiring a multi-stage array like some other filters.

6. CONCLUSION

In this research, a numerical analysis was conducted to evaluate and compare the performance of a novel Hybrid filter and a conventional Vortex Tube Separator (VTS) filter design with respect to their particle separation efficiency. The comparison between these two filters revealed several key findings. Firstly, the Hybrid VTS-IPS filter exhibited superior particle separation efficiency compared to the VTS filter, particularly for very fine particles with diameters of 2 μm and 5 μm. The Hybrid filter achieved separation efficiencies of up to 99%, whereas the VTS filter reached a maximum value of 47% for these particle diameters. Although both filters demonstrated good separation efficiency for fine particles, the Hybrid filter still outperformed the VTS filter. Moreover, for low velocities of $\boldsymbol{v \leq 7.5\ m/s}$, the maximum efficiencies for particle diameters of 20 μm and 25 μm were 88% and 95%, respectively, for the VTS filter, whereas the efficiency of the Hybrid filter reached 99%.

The effectiveness of the Hybrid filter in particle separation was further enhanced by the Hub geometry of the Internal Particle Separator (IPS) part of the filter, which caused a change in the direction of airflow and helped force the very fine particles out of the scavenging outlet. The separation efficiency was found to be dependent on the particle size, inlet velocity, and bypass value, with an increase in these factors leading to an increase in separation efficiency. For mixtures of particle sizes, the Hybrid filter demonstrated better particle separation compared to the VTS filter, achieving a separation efficiency of 94% compared to a maximum efficiency of 90% for the VTS filter.

Although the pressure drop in the VTS filter was found to be lower than that of the Hybrid filter, further optimization of the Hybrid filter could be performed to reduce the pressure drop while maintaining the high separation efficiency. Overall, the Hybrid filter design demonstrated superior particle separation performance and has the potential to be a promising candidate for various industrial applications.

ACKNOWLEDGEMENTS

The authors would like to acknowledge all the persons who helped us in this work, both in the fluid and energy laboratory at Ecole Militaire Polytechnique in Algiers and the mechanical department at Royal Military Academy in Brussels.

CONFLICT OF INTEREST

The authors declare that they have no competing interests.

AUTHORS CONTRIBUTION

S. Ghodbane: wrote the first version of the manuscript; contribute to the design and simulation; contributed to answering comments. A. Beniaiche: supervision; review and editing; contributed to answering comments. A. Belkallouche: supervision; contributed to design and simulation; review and editing. B. Jenssens: supervision; review and editing.

REFERENCES

Alqallaf, J., & Teixeira, J. A. (2022). Numerical study of effects of solid particle erosion on compressor and engine performance. *Results in Engineering*, 15, 100462. https://doi.org/10.1016/j.rineng.2022.100462

Barone, D., Loth, E., & Snyder, P. (2017). Influence of particle size on inertial particle separator efficiency. *Powder Technology*, 318, 177-185. https://doi.org/10.1016/j.powtec.2017.04.044

Bojdo, N. M. (2012*). Rotorcraft engine air particle separation.* The University of Manchester (United Kingdom).

Bojdo, N., & Filippone, A. (2012). A comparative study of helicopter engine air particle separation technologies.

Bojdo, N., & Filippone, A. (2017, September). *Conceptual and preliminary design of a hybrid dust filter for helicopter engines.* Conference: European Rotorcraft Forum At: Milan, Italy.

Connolly, B. J., Loth, E., & Smith, C. F. (2023). Efficiency of inertial particle separators. *Powder Technology*, 413, 118004. https://doi.org/10.1016/j.powtec.2022.118004

Cozier, A. D., Harned, K. E., Riley, M. A., Raabe, B. H., Sommers, A. D., & Pierson, H. A. (2015, November). *Additive manufacturing in the design of an engine air particle separator.* ASME International Mechanical Engineering Congress and Exposition, American Society of Mechanical Engineers. https://doi.org/10.1115/IMECE2015-51592

Crowe, C. T., Sommerfeld, M., & Tsuji, Y. (1998). Multiphase flows with particles and droplets, CRC Press, pp. 57–88.

Daldal, A. B. (2023). *Investigation of inertial particle separator from a broader perspective*. [Master's thesis, Middle East Technical University].

Dziubak, T. (2020). Experimental research on separation efficiency of aerosol particles in vortex tube separators with electric field. *Bulletin of the Polish Academy of Sciences: Technical Sciences*, 503-516. https://doi.org/10.24425/bpasts.2020.133385

Dziubak, T., Bąkała, L., Karczewski, M., & Tomaszewski, M. (2020). Numerical research on vortex tube separator for special vehicle engine inlet air filter. *Separation and Purification Technology*, 237, 116463. https://doi.org/10.1016/j.seppur.2019.116463

Elghobashi, S. (1994). On predicting particle-laden turbulent flows. *Applied Scientific Research*, 52(4), 309-329. https://doi.org/10.1007/BF00936835

Filippone, A., & Bojdo, N. (2010). Turboshaft engine air particle separation. *Progress in Aerospace Sciences*, 46(5-6), 224-245. https://doi.org/10.1016/j.paerosci.2010.02.001

Fluent, A. N. S. Y. S. (2019). *Ansys fluent theory guide 2019R3.*

Ghenaiet, A., & Tan, S. C. (2004, January). *Numerical study of an inlet particle separator.* In Turbo Expo: Power for Land, Sea, and Air (Vol. 41677, pp. 269-281). https://doi.org/10.1115/GT2004-54168

Gopalakrishnan, B. (2019). *Numerical analysis of multiphase flow through axial vortex tube cyclone separators.* E3S Web of Conferences, EDP Sciences.

Hamed, A., Tabakoff, W. C., & Wenglarz, R. V. (2006). Erosion and deposition in turbomachinery. *Journal of Propulsion and Power*, 22(2), 350-360. https://doi.org/10.2514/1.18462

Hobbs, J. R. (1983). U.S. Patent No. 4,389,227. Washington, DC: U.S. Patent and Trademark Office.

Jennings, S. G. (1988). The mean free path in air. *Journal of Aerosol Science*, 19(2), 159-166. https://doi.org/10.1016/0021-8502(88)90219-4

Milluzzo, J., & Leishman, J. G. (2010). Assessment of rotorcraft brownout severity in terms of rotor design parameters. *Journal of the American Helicopter Society*, 55(3), 32009-32009. https://doi.org/10.4050/JAHS.55.032009

Prinsloo, W. J., De Villiers, P., & Van Dijken, M. C. (1991). U.S. Patent No. 4,985,058. Washington, DC: U.S. Patent and Trademark office.

Saberi, s. (2014). *numerical model and analysis on performance of a straight-through swirl tube cyclone (Inertial Gas-Solid Separator).* [Doctoral dissertation, Concordia University].

Song, X., Xu, Z., Li, G., Pang, Z., & Zhu, Z. (2017). A new model for predicting drag coefficient and settling velocity of spherical and non-spherical particle in Newtonian fluid. *Powder Technology*, 321, 242-250. https://doi.org/10.1016/j.powtec.2017.08.017

Stallard, P. (1997). Helicopter engine protection. *Perfusion*, 12(4), 263-267. https://doi.org/10.1177/026765919701200410

Sommerfeld, M. (2017). Numerical methods for dispersed multiphase flows. *Particles in flows*, 327-

396. https://doi.org/10.1007/978-3-319-60282-0_6

Tabakoff, W., & Hamed, A. (1984, October). *Installed engine performance in dust-laden atmosphere*. Aircraft Design Systems and Operations Meeting.

Vallier, A. (2009). *Tutorial icolagrangianfoam/solidparticle.* Chalmers University of Technology, Goteborg, Sweden. Peer reviewed tutorial, Hakan Nilsson, CFD with OpenSource Software.

Van der Walt, J. P., & Nurick, A. (1995a). Erosion of dust-filtered helicopter turbine engines part I: basic theoretical considerations. *Journal of Aircraft*, 32(1), 106-111. https://doi.org/10.2514/3.56919

Van der Walt, J. P., & Nurick, A. (1995b). Erosion of dust-filtered helicopter turbine engines part II: erosion reduction. *Journal of Aircraft*, 32(1), 112-117. https://doi.org/10.2514/3.46690

Zhou, L., Wang, Z., & Shi, J. (2019). Optimization design of the integral inertial particle separator based on response surface method. *Journal of Applied Fluid Mechanics*, 13(1), 133-145. https://doi.org/10.29252/jafm.13.01.30186